A Low-Power, Battery-Free Tag for Body Sensor Networks

Citation: Mandal, S., L. Turicchia, and R. Sarpeshkar. “A Low-Power, Battery-Free Tag for Body Sensor Networks.” Pervasive Computing, IEEE 9.1 (2010): 71-77. © 2010, IEEE

Published Version: http://dx.doi.org/10.1109/mprv.2010.1

Publisher: Institute of Electrical and Electronics Engineers ; IEEE Computer Society

Permanent Link: http://hdl.handle.net/1721.1/61413

Version: Final published version: final published article, as it appeared in a journal, conference proceedings, or other formally published context

A Low-Power, Battery-Free Tag for Body Sensor Networks

A new tag for pervasive sensing applications consists of a custom integrated circuit, an antenna for radio frequency energy harvesting, and sensors for monitoring physiological parameters.

Soumyajit Mandal, Lorenzo Turicchia, and Rahul Sarpeshkar
Massachusetts Institute of Technology

With the world population aging rapidly, providing timely care for the elderly is becoming increasingly important. For instance, more than 5,000 people experience sudden cardiac arrest (SCA) every week in the US. The only definitive treatment for SCA is early defibrillation—no more than six minutes from arrest to first shock. The chance for survival drops 10 percent per minute without defibrillation, and today, more than 95 percent of SCA victims die.[1] In addition, in the US alone, approximately 2,000 infants die each year from sudden infant death syndrome (SIDS). Because a slow heart rate (bradycardia) is an important indicator of SIDS,[2] early detection could save many lives.

Wireless networks of context-aware, body-mounted sensors have come into prominence recently for providing timely care via pervasive patient monitoring.[3,4] However, to be effective, these systems should be unobtrusive, robust, and inexpensive. We've designed a wearable tag that can monitor multiple biomedical signals—heart sounds (phonocardiogram; PCG), electrical heart signals (electrocardiogram; EKG), blood oxygen saturation (photoplethysmogram; PPG), respiratory sounds,[5] blood pressure, and body temperature. The tag generates an alarm when it suspects a patient emergency. To quickly cover a large portion of the population at risk, we kept the tag affordable (less than US$2 each when manufactured in volume), disposable, small, and easy to use. Such tags would be useful for hospitals, facilities for infants and the elderly, and ordinary homes to detect and alert caregivers to possible problems including SCA and SIDS.

System Design

In this instantiation, we use sounds, not electrical signals, for heart monitoring—that is, PCG instead of EKG. PCG has three advantages over EKG. First, it doesn't require electrical contact with the body, which is often difficult with dry skin. Second, because the heart is the loudest organ in the body and easy to sense acoustically, PCG can use a very low-power, cheap microphone. Third, it requires little maintenance.

Alarm Types

Our tag uses multiple sensors to generate three types of alarms: disconnection from the body, device malfunction, and patient emergency. As Figure 1 shows, the device has two microphones, one facing up (away from the body) and the other down. The downward-facing microphone monitors heart sounds; the upward-facing one is usually switched off to save power, turning on only when the other microphone doesn't detect heart sounds. If, at this point, both microphones pick up similar environmental sounds, a *disconnection alarm* sounds because the tag is probably no longer near the skin. A *patient-emergency*

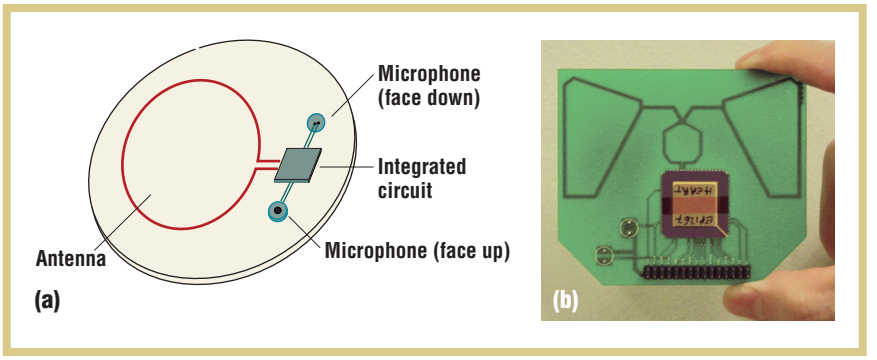

Figure 1. A simplified version of our patient-monitoring tag with two microphones and an antenna. (a) A conceptual view of the tag attached to a flexible, adhesive surface and (b) a photograph of the 800-MHz prototype that we tested. We estimate that product designers can halve the prototype's area by using a smaller package for the chip and an optimized antenna. In addition, the pins at the bottom of the prototype were for testing purposes and aren't necessary for a commercial system.

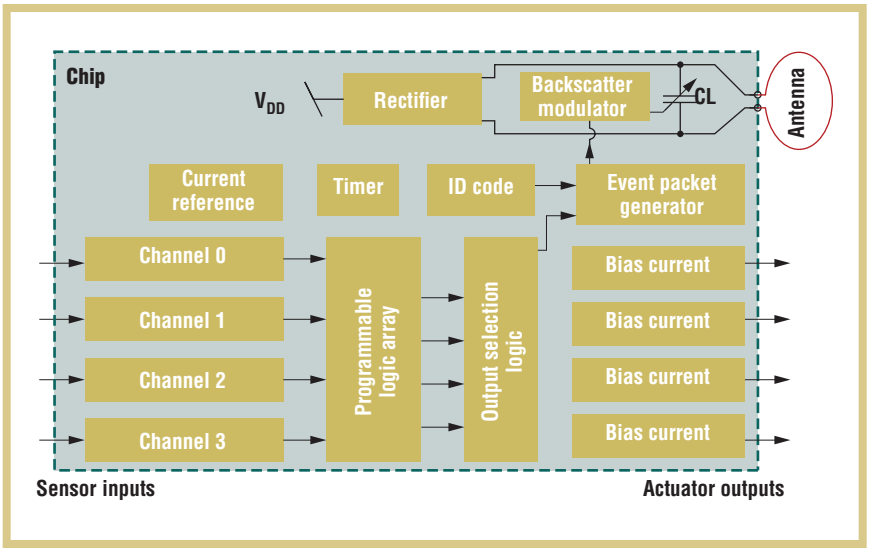

Figure 2. A block diagram of the low-power patient-monitoring chip. The chip accepts inputs from up to four sensors and powers up to four actuators. It harvests RF energy from the environment using an external antenna and uses backscatter modulation to send data to a remote base station.

alarm sounds if the downward-facing microphone doesn't pick up environmental sounds but the upward-facing one does, because in this case, the tag likely is still attached and the heart has stopped. If neither microphone picks up any sounds, the tag is probably malfunctioning, so a *device-malfunction alarm* sounds. Each tag contains a unique identification code; a fixed base station communicates with multiple tags and decides, on the basis of transmitted patient data, whether it should trigger an alarm.

Energy Harvesting

The tag contains a low-power integrated circuit that provides power-harvesting, sensing, and actuation capabilities. Figure 2 shows a block diagram of the chip. We designed it to be extremely low power by incorporating only minimally acceptable amounts of computation and signal processing; the fixed base station performs the more complex computations. The chip can harvest radiated radio frequency (RF) power,[6] making a low-cost, battery-free tag possible. A two-stage complementary metal-oxide semiconductor (CMOS) rectifier connects to the antenna[7] shown in Figure 1. The chip's input capacitance, C_L, resonates with the antenna's inductive input reactance at the operating frequency. The resultant L-type impedance match provides passive voltage gain that reduces the amount of RF power needed to overcome the rectifier's dead zone, thereby increasing operating range.

We designed the first rectifier stage with low-output impedance because it powers up external sensors, which typically consume much more power than the chip itself. The second stage, which provides a higher-impedance output, powers up the chip. Overvoltage protection circuits at the power supply and RF input nodes prevent large RF amplitudes from damaging the chip.

Path loss models predict the loss of radiated power density P_r (in W/m^2) with distance D from the transmitter. A simple version commonly used for modeling indoor environments recognizes two zones:

$$P_r \propto D^{-n_1} \text{ for } D \leq D_0$$

and

$$P_r \propto D^{-n_2} \text{ for } D > D_0,$$

where D_0, n_1, and n_2 are constants.[8] Typically, $n_1 \approx 2$, the free-space value, and n_2 varies between 2.5 and 4. The value of n_2 exceeds 2 because of RF absorption and reflection by environmental obstacles, such as furniture and people. We assumed the following conservative values: $D_0 = 5$ m, $n_1 = 2$, and $n_2 = 3.5$.

We developed a model that accurately

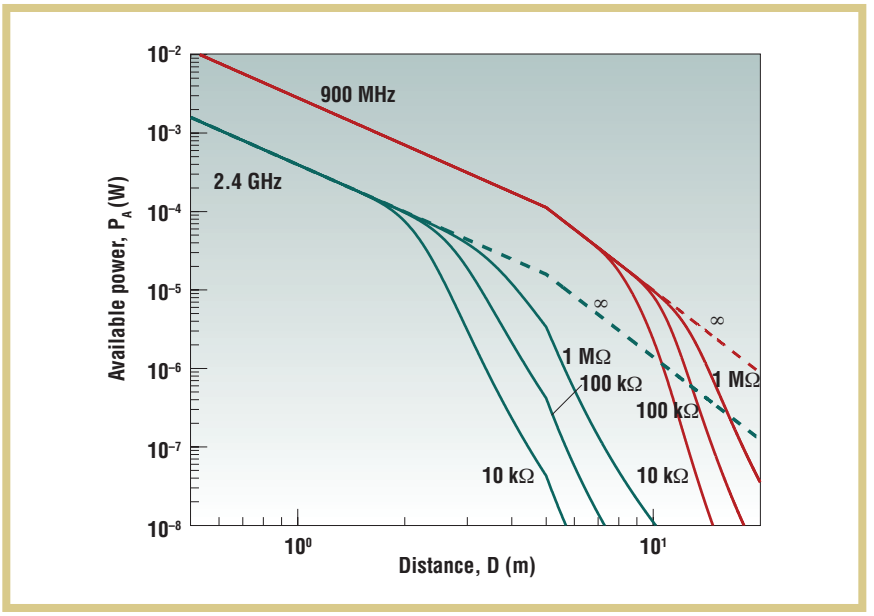

Figure 3. Theoretical limits on harvested radio frequency power as a function of distance from the transmitter. The graph shows P_A as a function of D at two popular RFID frequencies, 900 MHz and 2.4 GHz.

predicts our rectifier's output voltage as a function of available RF power and the output load (described in greater detail in "Low-Power CMOS Rectifier Design for RFID Applications"[7]). Combining the predicted path loss with this rectifier model gives us the power-harvesting limits shown in Figure 3, where P_A is the RF power that we can harvest at different distances from the transmitter. The graph assumes that the equivalent isotropic radiated power (EIRP) is 4 W, which is the maximum allowed for RFID applications in the US. It shows P_A as a function of D at two popular RFID frequencies: 900 MHz and 2.4 GHz. The main reason for going to higher operating frequencies is to reduce the antenna size.

The various curves in Figure 3 correspond to different rectifier-driven load resistances R_L. They decrease rapidly at greater distances because the received RF amplitude becomes smaller than the rectifier's dead zone. The power that the off-chip sensors consume—and not the chip itself—usually dominates the load resistance. For example, a microphone biased at 30 μA and 0.5 V (typical values used in our experiments) dissipates 15 μW, corresponding to an effective rectifier-driven load of R_L = 16.7 kΩ.[7]

The graph in Figure 3 predicts an operating range of approximately 12 m at 900 MHz and 3 m at 2.4 GHz. In practice, the reliable operating range will be somewhat smaller because some tags will be mistuned by their proximity to conductive and dielectric surfaces. In addition, we allow for transient drops in received RF power level (fades), which are ubiquitous in indoor environments because the received signal is the superposition of multiple

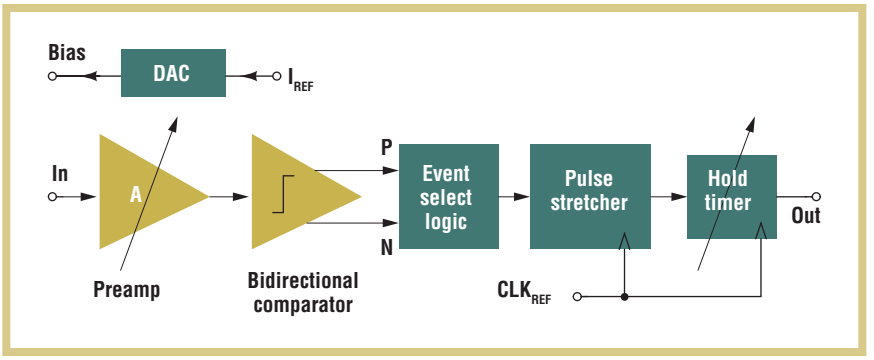

Figure 4. A single on-chip signal-processing channel. The channel contains a sensing path with a preamplifier, a comparator for detecting events, logic for rejecting unwanted events, and an actuation path that supplies bias current to an external sensor, such as a microphone.

waves with time-varying amplitude and phase. A single base station operating at 900 MHz is sufficient for a moderately sized room.

Signal-Processing Channels

Our chip contains four independent channels that can interface with various sensors. These channels' outputs are digital spikes, or *event signals*, which can combine in a flexible way using a programmable logic array (PLA) that can implement a variety of Boolean logic functions. Our PLA is a four-input, four-output design with an 8 × 8 AND plane and a 4 × 8 OR plane. It lets us implement any of the 2^{2^4} possible logic functions of four inputs for any of its four outputs in a programmable fashion. We can monitor these outputs individually, which lets us implement rudimentary sensor-fusion algorithms that combine multiple channels' outputs.

Programmable output selection logic multiplexes the four PLA outputs into a single signal that's transmitted to the base station as *event packets* containing the chip identification code and time stamps. Data is transmitted using *backscatter modulation*:[9] a 100-fF capacitor is added to or subtracted from

C_L to change the amount of RF power the tag scatters. Backscatter modulation is popular in passive RFID systems because it pushes all the complexity and power consumption to the base station; the tag remains simple and consumes little power.

Figure 4 shows a block diagram of a single channel. The preamplifier consists of a common-source stage with capacitive feedback; the feedback capacitor's size can vary between C_0 and 16 C_0 to set the gain. The amplifier rejects very low-frequency signals, which usually contain no useful information; the transfer function is band-pass with a low cut-in frequency (typically less than 1 Hz). It uses a nominal bias current of 10 nA and C_0 = 0.5 pF, resulting in a bandwidth that decreases from 12 kHz to 6 kHz as the gain increases from 1 to 16.

The comparator generates events whenever the amplifier's output voltage differs from its quiescent value by more than a fixed threshold voltage V_{th} = 80 mV. We use a matched copy of the amplifier (minus the capacitors) to determine the quiescent value. There are two event types: positive-going, in which the output voltage is larger than its quiescent value by V_{th} or more, and negative-going, in which it is smaller. The smallest input amplitude that triggers a spike decreases from V_{th} to V_{th}/16 (80 mV to 5 mV) as the preamplifier gain increases from 1 to 16.

The comparator output in each channel is connected to spike selection logic, which allows detection of positive-going spikes, negative-going spikes, both, or neither. A pulse-stretcher circuit follows this combinatorial block, adding hysteresis in the time domain to prevent noise from causing multiple transitions when the comparator detects an event. It also ensures that output spikes last long enough for at least one complete data packet to broadcast during each spike. The pulse-stretcher circuit is a digitally timed one-shot: it allows an incoming event edge to set its output high and a delayed version of this edge to reset it low.

The pulse stretcher is followed by a programmable hold-timer circuit. This circuit imposes a hold time T_{hold} after each spike, during which no new spikes can be generated. By placing an upper bound of $1/T_{hold}$ on the spiking rate, the hold timer greatly reduces the probability of timing collisions between different tags. The average value of T_{hold} can vary from 94 ms to 1.4 sec.

We designed a programmable DC current source for each channel. This current source can power up external sensors, such as microphones, and consists of an 8-bit binary-weighted current digital-analog converter (DAC) that can supply between 0.5 μA and 128 μA. To reduce power consumption, we designed the chip to operate on power supply voltages as low as 0.8 V for the core and 0.5 V for the programmable current sources.

An on-chip serial interface lets users program the PLA, the channel selection logic, the 16-bit chip identification code, and channel parameters such as sensor current, preamplifier gain, and hold time. The static power consumption with no external sensors is only 1.0 μW. The power consumption with sensors present depends on their bias currents, which are application dependent.

An on-chip serial interface lets users program the PLA, the channel selection logic, the 16-bit chip identification code, and channel parameters.

Experiments and Results

We performed three sets of experiments to test our tag's range, monitor the heart, and verify that we could locate our tag using acoustic time delays. We selected the WM-63PR, a small, cheap, and thin (6 mm in diameter and 1.3 mm thick) Panasonic omnidirectional electret condenser microphone in a plastic enclosure, as our primary sensor. Microphones are normally placed on the chest for monitoring heart activity; however, the microphone membrane can't vibrate freely if it's directly attached to the skin. So, we added a small air chamber (approximately 1 mm thick) below our sensor. The chamber has no vents, reducing the amount of ambient noise, but its diameter and shape have little effect on sound pickup.

To save power, we biased our microphone's internal buffer, which consists of a junction field effect transistor (JFET), at much lower currents than recommended by the manufacturer. In this regime, the JFET is unsaturated and acts as a voltage-controlled resistor, making signal gain proportional to the bias current I_{bias}. By varying I_{bias} with the on-chip DAC, we can trade sensitivity for bandwidth and power consumption.[10] In practice, we save considerable amounts of power because heart sounds are relatively loud and low in bandwidth, typically 20 to 250 Hz.

Operating Range

In a cluttered laboratory environment, we were able to obtain 15 μW of output power at a distance of 3.1 m from an RF source broadcasting 800 mW EIRP at 800 MHz. This is enough to run the chip and one microphone at a typical bias current of 30 μA. Increasing the transmit power to the allowed maximum of 4 W gives us a free-space range of 7 m. We can further increase the operating range by a factor of approximately 1.4 by using a smaller package for the chip.[7] A circularly polarized transmitter antenna makes the power the tag receives less sensitive to

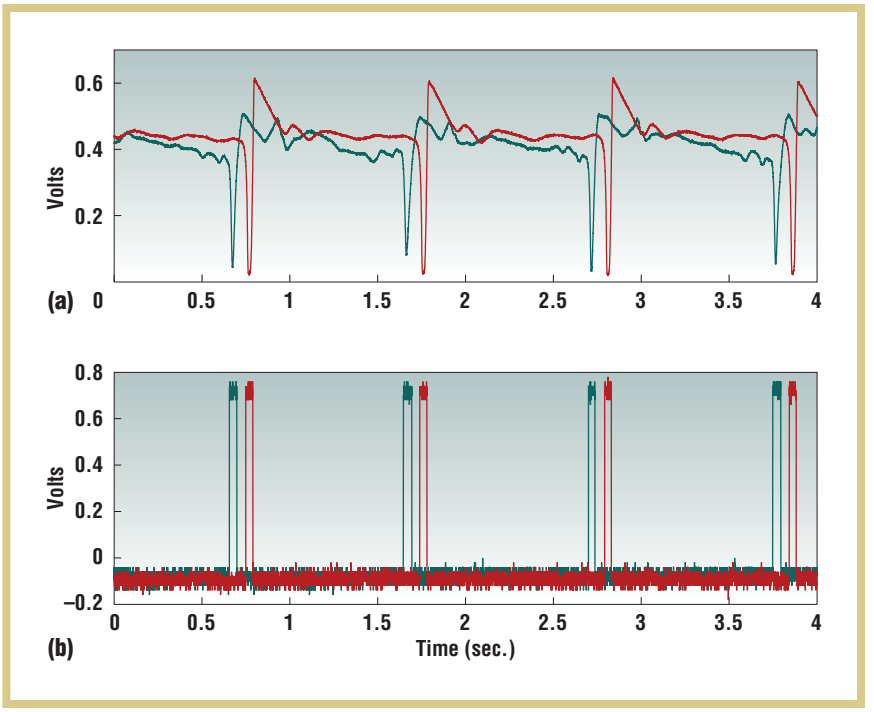

Figure 5. Phonocardiogram (PCG) waveforms. We simultaneously measured PCG at a subject's neck (green line) and wrist (red line) using two microphones and two signal-processing channels on our chip. Graph (a) shows the preamplifier's analog output in each channel, and graph (b) shows the final digital event, or spike, that each channel generates.

propagation barriers and its own spatial orientation.

The tag's operation was largely unaffected by the presence of the human body up to approximately 1 cm from the skin. The received power decreased sharply for smaller separations. Also, to operate normally, the microphone mustn't touch the skin. We solved both problems by backing the tag with dielectric foam approximately 1 cm thick. At 3 m from the source, the presence of another person directly between the source and the tag had almost no effect on received power, presumably because of multipath effects. Finally, the tag continued to operate at 2 m when the user wasn't facing the transmitter or was lying, tag downward, on the floor.

Monitoring the Heart

In all our heart-monitoring experiments, we biased microphones using on-chip current sources operating on a 0.5 V supply. In the first experiment, we connected two microphones to channels on the chip and attached these to the subject's neck and wrist, where we expected a strong pulse. We biased each microphone at 30 μA and set the preamplifier gain to 8. In other successful experiments, we placed the sensor at its default position, the chest. In this position, heart sounds are louder, further reducing the microphone bias current.

Figure 5 shows the measured PCG waveforms. The waveform at the wrist is delayed relative to that at the neck by approximately 95 ms because of the time the systolic pulse takes to propagate down the arm. This delay can provide information about blood pressure.[11] The systolic upsurge in blood pressure and consequent dilation of the arteries cause each large negative spike. The high-frequency components in conventional PCG waveforms are almost completely absent in these recordings for two reasons. First, the coupling between the skin and the microphone is a low-pass filter. Second, because we were interested mainly in heart-rate information, which resides in the loud, low-frequency PCG components (10 to 80 Hz), we deliberately kept microphone sensitivities low by reducing their bias currents.

In another experiment, we combined the wrist microphone, still biased at 30 μA, with an external pulse oximeter[12] connected to another channel. We attached the oximeter, which measures the blood's oxygen saturation level, to the subject's index finger. Pulse oximeters illuminate the skin with a light source, such as a light-emitting diode (LED), and measure the amount of light either transmitted or reflected to a sensor, such as a photodiode. The amount of detected light varies with time as the arteries contract and expand during the cardiac cycle. The resulting recording, known as a PPG, can be used to infer oxygen saturation level. For simplicity, we used an off-the-shelf infrared LED light source and a Texas Instruments OPT101 photosensor to measure the PPG. The OPT101 consisted of a photodiode and transimpedance amplifier integrated into a single package, and its output fed into our chip.

Figure 6 shows measured PCG and PPG waveforms. The peaks in the PPG waveform align with the negative spikes in the PCG because we recorded from adjacent locations. The pulse propagation delay from the wrist to the finger is small.

Tracking Location

Location awareness can improve response time to the tag's audio alarms by guiding caregivers directly to the patient.[13] Caregivers can infer patient movement patterns by monitoring location versus time; this additional information can improve the system's robustness and diagnostic capabilities. In this experiment, we localized a tag in a room via acoustic time-of-flight

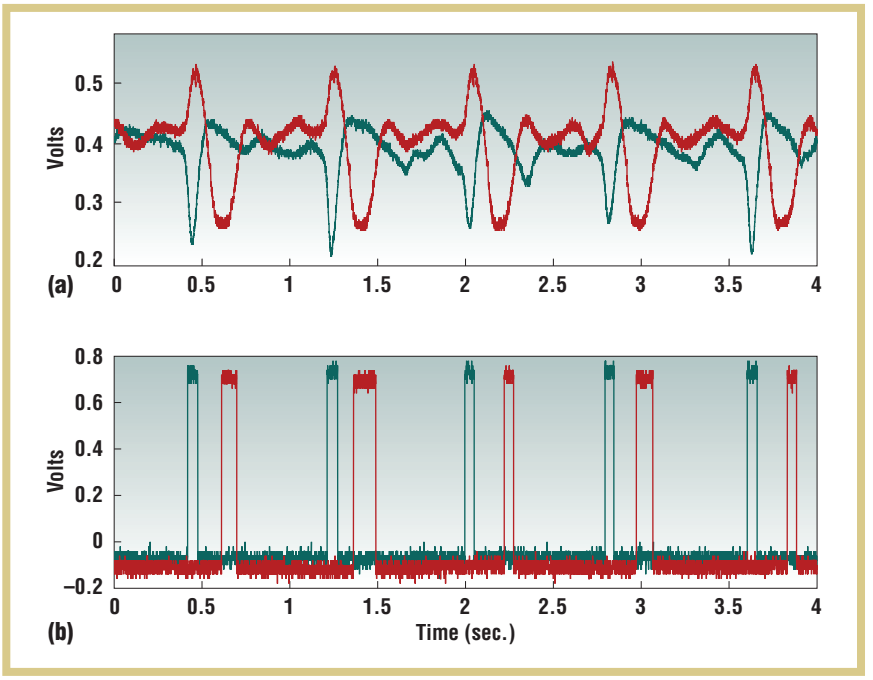

Figure 6. Two different ways to monitor the heart. We simultaneously measured the PCG from a subject's wrist (green line) and the photoplethysmogram (PPG) from the subject's fingertip (red line) using two signal-processing channels on our chip. Graph (a) shows the preamplifier's analog output within each channel, and graph (b) shows the final digital event, or spike, that each channel generates.

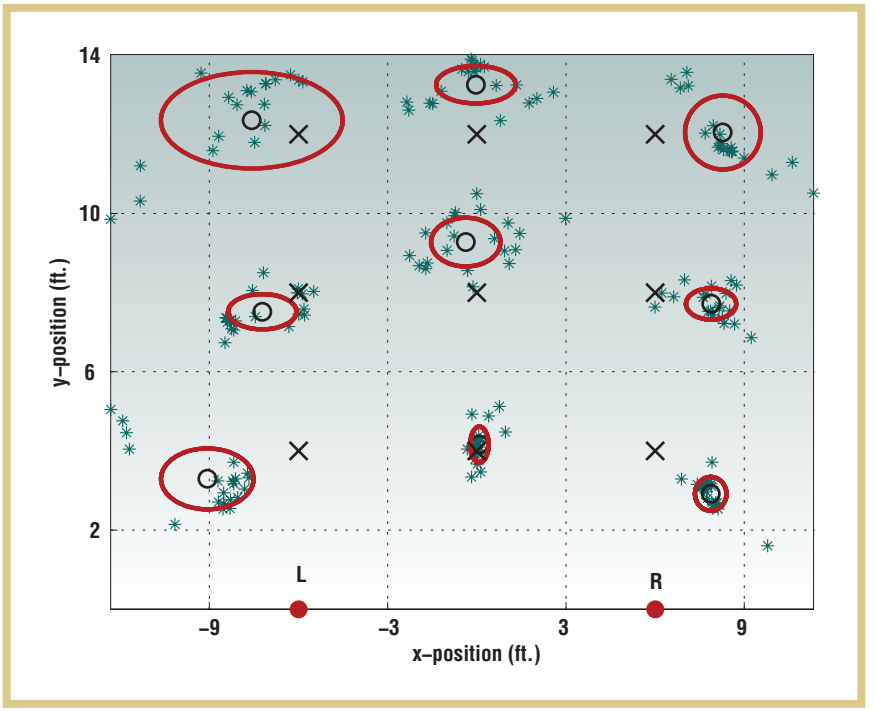

Figure 7. Localization in two dimensions using acoustic time delays. We measured data points (*), mean positions (o), and standard-deviation ellipses for nine tag locations. Actual positions (×) and the two speakers (●) are also marked.

measurements[14,15] using a single microphone attached to the chip and two speakers (L and R) placed a distance d apart. By measuring the time delays t_1 and t_2 between each speaker and the microphone, we located the tag's position in two dimensions.

We biased the microphone at 128 μA and cascaded preamplifiers from two channels to give a total gain of $8 \times 12 = 96$. We placed small speakers $d = 12$ ft. apart and programmed them to transmit 100 ms tone bursts at 230 Hz. To minimize audibility and attenuation with distance, we kept the burst frequency as low as possible but were limited by our small speakers' poor low-frequency response. We spaced the bursts 400 ms apart to ensure that all echoes from the first burst would die down before the second one arrived. The measured sound level at the center of the room with either speaker on was 87 dB SPL (sound pressure level), which is loud enough to serve as an alarm signal. We performed the experiment in a realistically noisy indoor environment (49 dB SPL, a typical quiet room being 40 dB SPL) that included sound propagation barriers in the form of furniture and people.

We estimated the propagation times t_1 and t_2 from the speaker to the tag by using a simple threshold-based algorithm to measure the time between the onset of each burst and the first spike the chip detects. By using the first spike, we measured the time delay corresponding to the shortest path—that is, line of sight. The microphone's distances from each speaker are given by $d_1 = ct_1$ and $d_2 = ct_2$, where c is the speed of sound in air—1,130 ft./sec.

Figure 7 shows the localization data for nine different tag positions and 20 trials. The average standard deviation in the measured positions was 1.4 ft. (0.43 m), and the average error between the measured and actual positions was 1.97 ft. (0.6 m). One significant source of error is the tag's signal detection delay—it increases with distance from the speaker and contributes approximately

1 ft. (0.3 m) of localization error at the farthest positions.

Our system's current accuracy already provides important information about the patient's location. For example, we can distinguish between the bed, a chair, and the bathroom. We can increase localization accuracy if necessary by using louder sounds or a higher transmission frequency to improve timing precision. We can also extend the system to three dimensions by adding a third speaker. Finally, we can localize our tags to particular rooms by determining which RF transmitter powers them up. This information lets localization accuracy degrade gracefully if the audio scheme fails.

The audio alarm and localization technique is quite general and can extend to other wireless sensor applications. For example, it can form the basis for sensor-fusion algorithms in which the audio alarm can activate sensors—such as video cameras that provide high-bandwidth information—when it detects abnormal events. This reduces the amount of information that a human operator needs to monitor continuously, and also allows power-hungry sensors to be turned off most of the time. We plan to begin field trials of our technology in a relatively well-monitored environment, such as an assisted-living center, and later extend these trials to less controlled environments, such as private homes. P

REFERENCES

1. J.J.M. de Vreede-Swagemakers et al., "Out-of-Hospital Cardiac Arrest in the 1990s: A Population-Based Study in the Maastricht Area on Incidence, Characteristics and Survival," *J. Am. College of Cardiology*, vol. 30, no. 6, 1997, pp. 1500–1505.
2. R.G. Meny et al., "Cardiorespiratory Recordings from Infants Dying Suddenly and Unexpectedly at Home," *Pediatrics*, vol. 93, no. 1, 1994, pp. 44–49.
3. G.-Z. Yang, ed., *Body Sensor Networks*, 1st ed., Springer, 2006.
4. *Proc. Int'l Workshop Wearable and Implantable Body Sensor Networks* (BSN 06), IEEE CS Press, 2006.
5. *IEEE Eng. in Medicine and Biology Magazine*, vol. 26, no. 1, 2007, pp. 15–70.
6. J.R. Smith et al., "A Wirelessly-Powered Platform for Sensing and Computation," *Proc. 8th Int'l Conf. Ubiquitous Computing* (Ubicomp 06), Springer, 2006, pp. 495–506.
7. S. Mandal and R. Sarpeshkar, "Low-Power CMOS Rectifier Design for RFID Applications," *IEEE Trans. Circuits and Systems I*, vol. 54, no. 6, pp. 1177–1188.
8. K.S. Leong, M.L. Ng, and P.H. Cole, "Operational Considerations in Simulation and Deployment of RFID Systems," *Proc. 17th Int'l Zurich Symp. Electromagnetic Compatibility*, IEEE Press, 2006, pp. 521–524.
9. K. Finkenzeller, *RFID Handbook: Fundamentals and Applications in Contactless Smart Cards and Identification*, 2nd ed., John Wiley & Sons, 2003.
10. S. Mandal, L. Turicchia, and R. Sarpeshkar, "A Battery-Free Tag for Wireless Monitoring of Heart Sounds," *Proc. Int'l Workshop Wearable and Implantable Body Sensor Networks* (BSN 09), IEEE CS Press, 2009, pp. 201–206.
11. J.C. Bramwell and A.V. Hill, "The Velocity of the Pulse Wave in Man," *Proc. Royal Soc. London*, Series B, vol. 93, no. 652, pp. 298–306.
12. J.G. Webster, *Design of Pulse Oximeters*, 1st ed., Taylor & Francis, 1997.
13. M. Hazas, J. Scott, and J. Krumm, "Location-Aware Computing Comes of Age," *Computer*, vol. 37, no. 2, pp. 95–97.
14. X. Bian, G.D. Abowd, and J.M. Rehg, "Using Sound Source Localization in a Home Environment," *Pervasive Computing*, LNCS 3468, Springer, 2005, pp. 19–36.
15. J. Scott and B. Dragovic, "Audio Location: Accurate Low-Cost Location Sensing," *Pervasive Computing*, LNCS 3468, Springer, 2005, pp. 1–18.

the AUTHORS

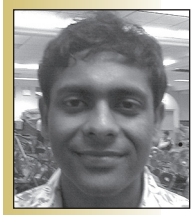

Soumyajit Mandal is a postdoctoral associate in the Department of Electrical Engineering and Computer Science at the Massachusetts Institute of Technology (MIT). His research interests include analog and hybrid computation, nonlinear dynamics, biochemical networks, and antennas. Mandal has a PhD in electrical engineering from MIT. He's a member of the IEEE. Contact him at soumya@mit.edu.

Lorenzo Turicchia is a research scientist in MIT's Department of Electrical Engineering and Computer Science. His main research interests are nonlinear signal processing, such as audio and biomedical signal processing, and bioelectronics. Turicchia has a PhD in computer science from the University of Udine. Contact him at turic@mit.edu.

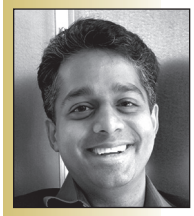

Rahul Sarpeshkar is an associate professor in MIT's Department of Electrical Engineering and Computer Science. His research interests include analog and mixed-signal integrated circuit design, biomedical systems, ultra-low-power circuits and systems, biologically inspired circuits and systems, molecular biology, neuroscience, and control theory. Sarpeshkar has a PhD from the California Institute of Technology. He's a senior member of the IEEE. Contact him at rahuls@mit.edu.